

# Design of Dual Band MIMO Antenna with Rhombus Shape for Wireless Applications

Chirukuri Naga Phaneendra and Ketavath Kumar Naik\*

*Antenna Research Laboratory, Department of Electronics and Communication Engineering  
Koneru Lakshmaiah Education Foundation (KLEF) deemed to be University, Vaddeswaram, Guntur 522502, India*

**ABSTRACT:** In this paper, a compact quad-port Rhombus-Shaped MIMO Patch (RSMP) antenna with a complete ground structure has been designed for dual-band wireless applications. The RSMP antenna has a common patch configuration and resonates at 12.9 GHz and 16.5 GHz with the reflection coefficients of  $-17$  dB and  $-25.7$  dB, respectively. A rhombus-shaped slot is etched from the patch to generate dual-band frequencies. Microstrip feed lines are connected to the common patch and are used to improve the overall performance of the RSMP antenna. The RSMP antenna has gains of 9.62 dBi and 9.98 dBi at resonating frequencies. The bandwidths of the proposed MIMO antenna model are 300 MHz and 350 MHz, respectively. The proposed RSMP antenna model was fabricated and tested with the vector network analyzer Keysight N9917A for validation. The simulated and measured results for the gain, reflection coefficients, surface current distribution, radiation pattern, envelope correlation coefficient (ECC), diversity gain (DG), total active reflection coefficient (TARC), and channel capacity loss (CCL) are compared, and they are agreed well for wireless applications at Ku-band for broadcasting communications.

## 1. INTRODUCTION

Nowadays, wireless communication systems play a very important role in our everyday lives. In traditional communication systems, using discrete antenna elements has limitations to support the increased demands of higher data rates, improved system reliability, and enhanced spectral efficiency. Multiple-input multiple-output (MIMO) antenna systems have emerged as a key technology to address these challenges. MIMO is a technology that allows several data streams to be transmitted and received concurrently over multiple antennas, improving performance in wireless communication systems. It leverages the spatial domain to improve the capacity, reliability, and overall quality of wireless communication systems.

According to the literature review, MIMO antennas have received more attention than conventional antennas in wireless communication systems, because it has better efficiency, good diversity performance, low multipath fading, and better reliability. In [1], dual-band dual-polarized antennas are proposed to improve bandwidth and isolation. To get the polarization diversity in the MIMO antennas [2], a rhombus-shaped patch antenna with a Y-shaped feeding technique is proposed. A fractal rhombus-shaped antenna is proposed for ultra-wideband (UWB) applications [3]. Due to the structure, the isolation between the elements is reduced. In [4], a rhombus-shaped slot antenna is proposed for wireless applications. According to [5], the Ku-band patch dipole and Ka-band microstrip patch radiating elements are constructed for beam scanning applications. In [6, 7], quasi-isotropic radiation patterns are produced with the help of flexible material. Still, some MIMO characteristics need to be improved to improve the performance of the pro-

posed antenna. A rhombus-shaped patch antenna with different slots is proposed to produce better isolation [8]. A multi-slotted patch antenna along with a rhombus-shaped slot is proposed to study the effect of an etched patch [9, 10].

Due to the limited space available in communication portable devices, there is requirement to install several elements at both ends of wireless system [11]. The etching of varied shapes and slots on microstrip patch antenna with different substrate materials creates wideband properties [12, 13]. A coplanar waveguide-powered, flexible, interconnected 4-port MIMO antenna are intended for ultra-wideband, X, and Ku applications [14, 15]. Isolation is a crucial MIMO antenna characteristic. In [16], electronic band gaps and hairpin-shaped, faulty ground construction are utilized. To improve the gain in [17], metamaterials are used in the form of split-ring resonators. Cross-dipole antennas [18] are used to reduce mutual decoupling. In [19, 20], a triangle-shaped antenna is used for multi-band applications.

In this paper, a quad-port rhombus-shaped MIMO patch antenna with a complete ground structure is designed for wireless applications. The RSMP antenna resonates at 12.9 GHz and 16.5 GHz with a bandwidths of 300 MHz (12.77 GHz to 13.07 GHz) and 350 MHz (16.31 GHz to 16.66 GHz). The rhombus-shaped common patch with a rhombus-shaped slot is considered to enhance both gain and reflection coefficients.

## 2. ANTENNA STRUCTURE

A quad-port rhombus-shaped MIMO patch (RSMP) antenna with a rhombus-shaped slot is presented in this paper. The RSMP antenna is fabricated on Kapton polyimide substrate material. The proposed substrate has a dielectric constant of 3.5

\* Corresponding author: Ketavath Kumar Naik (kumarvrt@gmail.com).

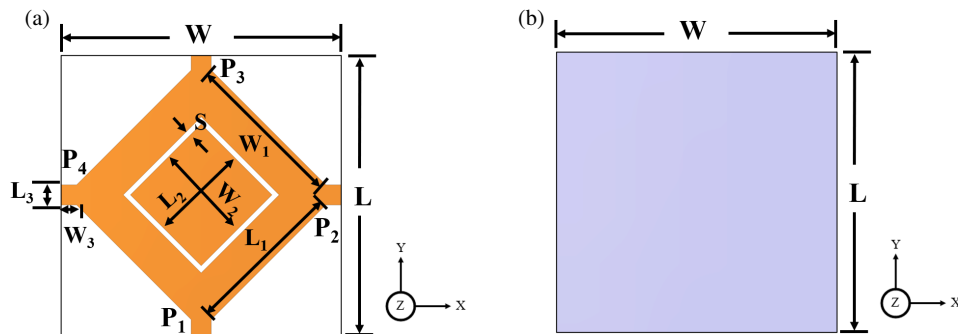


FIGURE 1. Physical layout of the RSMP antenna. (a) Top view. (b) Bottom view.

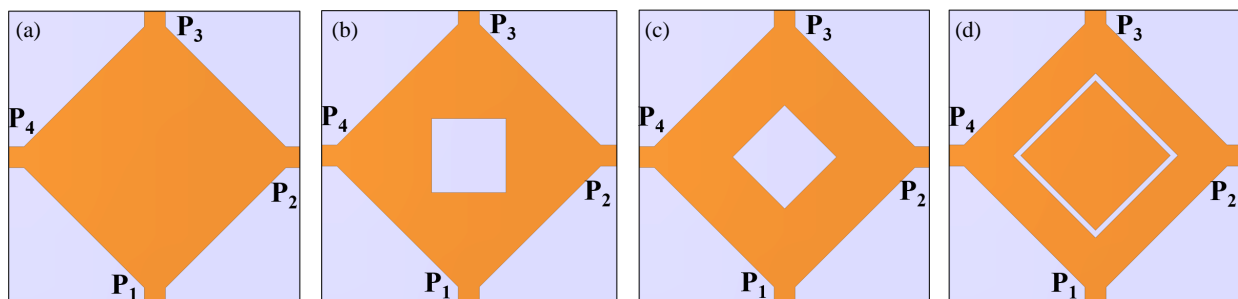


FIGURE 2. Evaluation process of the proposed MIMO antenna, (a) Ant. 1, (b) Ant. 2, (c) Ant. 3 and (d) Ant. 4.

TABLE 1. Optimized parametric values of RSMP antenna.

Parameters	Value (mm)	Parameters	Value (mm)	Parameters	Value (mm)
$L$	28	$W_1$	18	$L_3$	2
$W$	28	$L_2$	10	$W_3$	2
$L_1$	18	$W_2$	10	$S$	0.5

and a loss tangent of 0.008. The dimensions of substrate are  $L \times W \text{ mm}^2$ , with a height of 0.07 mm. The physical layout of the RSMP antenna is depicted in Fig. 1.

The ports of RSMP antenna are called as  $P_1$ ,  $P_2$ ,  $P_3$ , and  $P_4$  and shown in Fig. 1. From Fig. 1, the dimensions of the rhombus-shaped patch are  $L_1$  and  $W_1$  along the  $X$ -axis and  $Y$ -axis, with a height of 0.01 mm. The rhombus-shaped slot with width ‘ $S$ ’ is etched from the common radiating patch. The RSMP antenna has four ports; therefore, four microstrip feed lines are used for the excitation of RSMP antenna. Feed line length and width ( $L_3$  and  $W_3$ ) are united with proposed rhombus-shaped patch with an input impedance of  $50 \Omega$ . One side of the substrate has a patch, and the other side of the substrate is coated with a copper material with a height of 0.01 mm to act as a ground plane. In this proposed RSMP antenna structure, a complete ground plane is considered. The optimized parameter values of the RSMP antenna are listed in Table 1.

### 3. DESIGN PROCEDURE AND ANALYSIS

#### 3.1. Design Process of Proposed Antenna

The evaluation of RSMP antenna is illustrated step by step in Fig. 2. The evaluation process for RSMP antenna consists of a

total of four steps. In all these steps, the full ground plane structure and microstrip feed line techniques are commonly used. In the first step, a basic four-port rhombus-shaped patch antenna with a full ground structure is considered as Ant.1, shown in Fig. 2(a). There is no response found within the band, which is explained in Fig. 3.

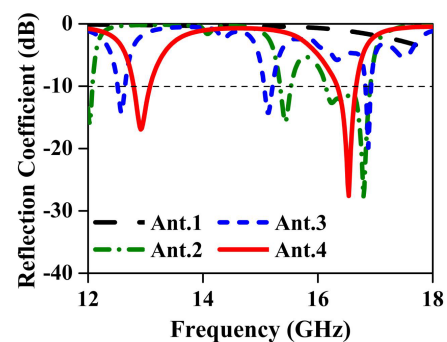
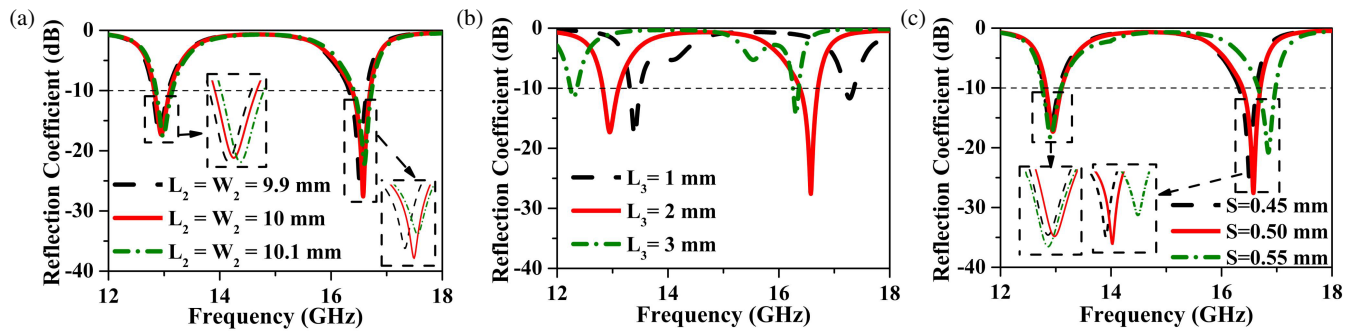


FIGURE 3. Evaluation process of RSMP antenna with respect to reflection coefficient.

After that, in the second step a square-shaped slot is etched from the patch, and it is considered as Ant.2, shown in Fig. 2(b). Ant.2 resonates at 15.4 GHz and 16.7 GHz with reflection

**TABLE 2.** Quantitative analysis of RSMP antenna.

Iteration	operating frequency (GHz)	Bandwidth (MHz)	Gain (dBi)	Reflection Coefficient (dB)
Ant-1	-	-	-	-
Ant-2	15.4	200	2.71	-15
	16.7	700	4.24	-27
Ant-3	12.5	100	4.17	-14
	15.1	200	5.27	-14
	16.8	200	6.45	-19
Ant-4	12.9	300	9.62	-17
	16.5	350	9.98	-27

**FIGURE 4.** Parametric analysis. (a) Parameter  $L_2$  and  $W_2$ . (b) Parameter  $L_3$ . (c) Parameter  $S$ .

coefficients of  $-15$  dB and  $-27$  dB. However, the gain and impedance bandwidths of Ant.2 are 200 MHz, 700 MHz, 2.71 dBi, and 4.24 dBi. In the third step, the square-shaped slot is converted into a rhombus-shaped slot with an angle of 45 degrees on the radiating patch considered as Ant.3, as shown in Fig. 2(c). Ant. 3 resonates at three operating frequencies: 12.5 GHz, 15.1 GHz, and 16.8 GHz, with minimum reflection coefficients of  $-14$  dB,  $-14$  dB, and  $-19$  dB. However, Ant.3 generates impedance bandwidths and gains of 100 MHz, 200 MHz, 200 MHz, 4.17 dBi, 5.27 dBi, and 6.45 dBi at three operating frequencies, but the reflection coefficient is very minimal. So, finally, to improve the reflection coefficient, impedance bandwidth, and gain, Step 4 is designed.

In the final step, the rhombus-shaped patch is added within the slot of Ant.3, and it is considered as Ant.4 shown in Fig. 2(d). Ant.4 resonates at two frequencies, 12.9 GHz and 16.5 GHz, to produce dual narrow bandwidths of 300 MHz and 350 MHz with reflection coefficients of  $-17$  dB and  $-27$  dB, respectively. Also, Ant.4 has maximum peak gains of 9.62 dBi and 9.98 dBi, which are better than the remaining steps of the design process. Hence, we consider Ant.4 as the proposed antenna. Fig. 3 shows the design and evaluation of the RSMP antenna in terms of the reflection coefficient. Table 2 explains the quantitative analysis of RSMP antenna evaluation.

### 3.2. Parametric Analysis

The parametric analysis helps to understand how the proposed RSMP antenna goes through various design steps. There are total nine parameters used in the design process. All the param-

eters are analyzed, but for brevity, some of them are presented in this paper and shown in Fig. 4.

To know the impact of parameter on the overall performance of an RSMP antenna, the antenna characteristics like impedance bandwidth, reflection coefficient, and gain are considered. From Fig. 4(a), it is clear that parameters  $L_2$  and  $W_2$  (inner patch dimensions) are varied from 9.9 mm to 10.1 mm with a step size of 0.1 mm. The effect of parameter on performance of RSMP antenna is explained in Fig. 4(a). The optimum results are obtained when we consider 10 mm. Hence, the optimum values of  $L_2$  and  $W_2$  are 10 mm. The effect of  $L_3$  (feed line length) is analyzed and explained in Fig. 4(b). The analysis of parameters is carried out, and  $L_3$  is 1 mm, 2 mm, and 3 mm. When  $L_3$  is equal to 1 mm and 3 mm, only a single band is generated. The dual band characteristics are obtained when we consider  $L_3 = 2$  mm. Hence, we consider the optimum value of  $L_3$  is 2 mm. To know the impact of  $S$  parameter (rhombus shaped slot width), it is varied from 0.45 mm, 0.5 mm, and 0.55 mm shown in Fig. 4(c). When  $S$  is 0.45 mm and 0.55 mm, the bandwidth is the same for both the lower and upper bands, but the reflection coefficient is less. The optimum results are obtained at  $S = 0.5$  mm. Hence, the optimum value of  $S$  is 0.5 mm.

### 3.3. MIMO Antenna Parameters

*Envelope Correlation Coefficient (ECC):* ECC measures the degree of similarity between the received signals in a fading environment. Ideally, ECC is zero. However, the accepted practical value of ECC should be  $\leq 0.5$ . Port 1 ( $P_1$ ) is considered

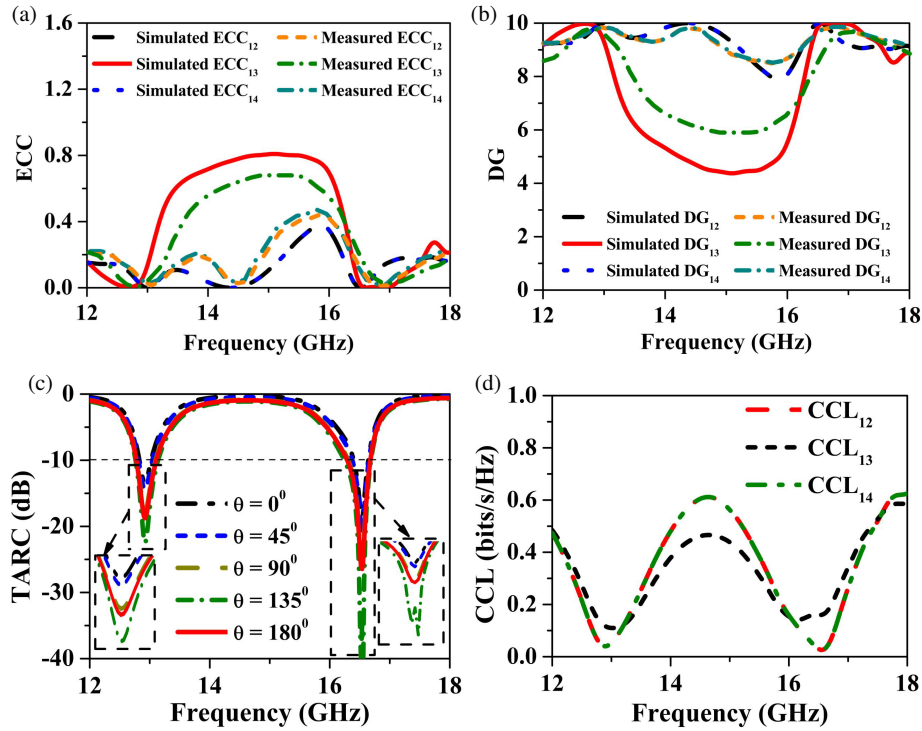


FIGURE 5. MIMO parameters, (a) ECC, (b) DG, (c) TARC, (d) CCL.

for computing all MIMO parameters. ECC can be calculated by using mathematical Equation (1). The ECC values of RSMP antenna are shown in Fig. 5(a).

$$\rho_e = \frac{|\iint_{4\pi} [F_{porti}(\theta, \varphi) * F_{portj}(\theta, \varphi)] d\Omega|^2}{\iint_{4\pi} |F_{porti}(\theta, \varphi)|^2 d\Omega \iint_{4\pi} |F_{portj}(\theta, \varphi)|^2 d\Omega} \quad (1)$$

where  $F_{porti}$  and  $F_{portj}$  indicate field radiation patterns of RSMP antenna at different ports. Here, Port 1 ( $P_1$ ) is considered for computing the MIMO parameters. So,  $i = 1$  and  $j = 2, 3, 4$  are port numbers.  $\theta$  and  $\varphi$  are the elevation and azimuth angles of field radiation pattern.

**Diversity Gain (DG):** The ideal value of DG is 10 dB. However, the practical value of more than 9 dB is accepted. This can be calculated by using mathematical Equation (2). The DG values of RSMP antenna are shown in Fig. 5(b).

$$DG = 10\sqrt{1 - [ECC]^2} \quad (2)$$

**Total active reflection coefficient (TARC):** TARC is defined as the ratio of the square root of total reflected power divided by the square root of total incident power. TARC at different values of  $\theta$  is measured and shown in Fig. 5(c). The TARC at the N-port antenna can be calculated by using Equation (3).

$$\Gamma_a^t = \frac{\sqrt{\sum_{i=1}^N |b_i|^2}}{\sqrt{\sum_{i=1}^N |a_i|^2}}, \quad (3)$$

where  $a_i$  is the incident signal, and  $b_i$  is the reflected signal.

**Channel capacity loss (CCL):** The CCL of the proposed antenna is calculated, and that value is  $< 0.4$  bits/sec/Hz for the entire band, which is shown in Fig. 5(d). The measured CCL is calculated by using the following equations:

$$CCL = -\log_2 \det(\psi^R) \quad (4)$$

where  $\psi^R$  is the correlation matrix at the receiver antenna system. That can be written as

$$\psi^R = \begin{bmatrix} \phi_{11} & \phi_{12} & \phi_{13} & \phi_{14} \\ \phi_{21} & \phi_{22} & \phi_{23} & \phi_{24} \\ \phi_{31} & \phi_{32} & \phi_{33} & \phi_{34} \\ \phi_{41} & \phi_{42} & \phi_{43} & \phi_{44} \end{bmatrix} \quad (5)$$

where,

$$\phi_{ii} = 1 - (|S_{ii}|^2 + |S_{ij}|^2) \text{ and } \phi_{ij} = -(S_{ii}^* S_{ij} + S_{ji}^* S_{ij}) \quad (6)$$

The simulated and measured envelope correlation coefficients, diversity gains (DGs), TARCs, and CCLs are calculated and shown in Fig. 5. These results show the values of  $ECC < 0.2$ ,  $DG > 9.5$  dB, and  $CCL < 0.4$  bits/sec/Hz within the frequency band, and they are accepted values for wireless applications.

The simulated and measured values of all S-parameters are calculated, but for brevity, here only port 1 analysis ( $S_{11}, S_{12}, S_{13}, S_{14}$ ) is considered and shown in Fig. 6. Due to the symmetrical structure of all ports, some of the graphs are overlapped. From Fig. 6(a), the resonant frequencies and impedance bandwidths of the simulated and measured results are almost the same, with a slight deviation in the reflection coefficient due to connecting wires and environmental conditions.

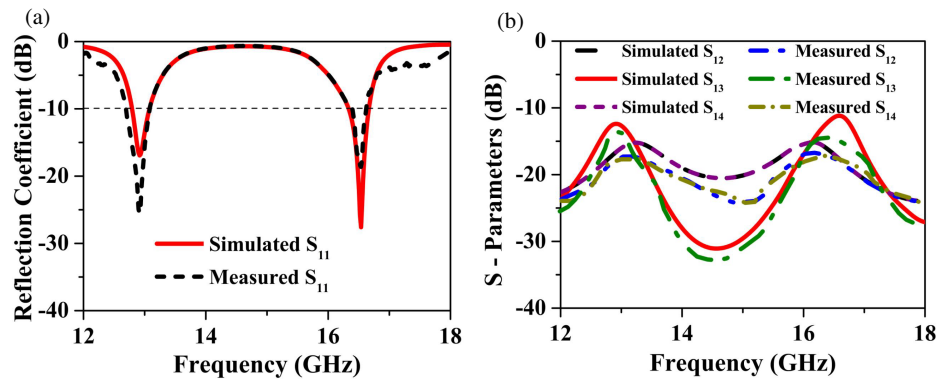


FIGURE 6. Simulation and measured values of (a)  $S_{11}$ , (b)  $S_{12}$ ,  $S_{13}$  and  $S_{14}$ .

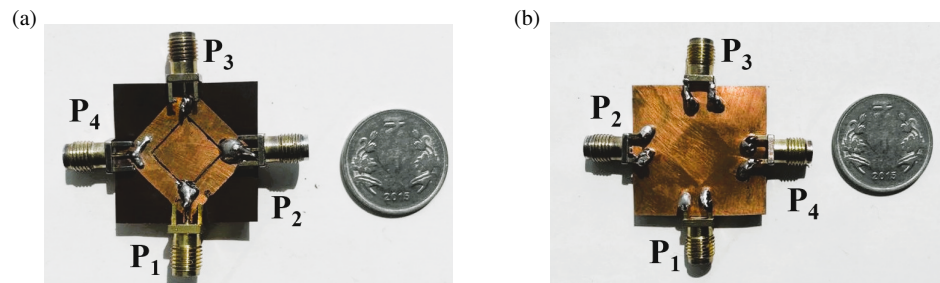


FIGURE 7. Fabricated prototype of proposed MIMO antenna model. (a) Top view. (b) Bottom view.

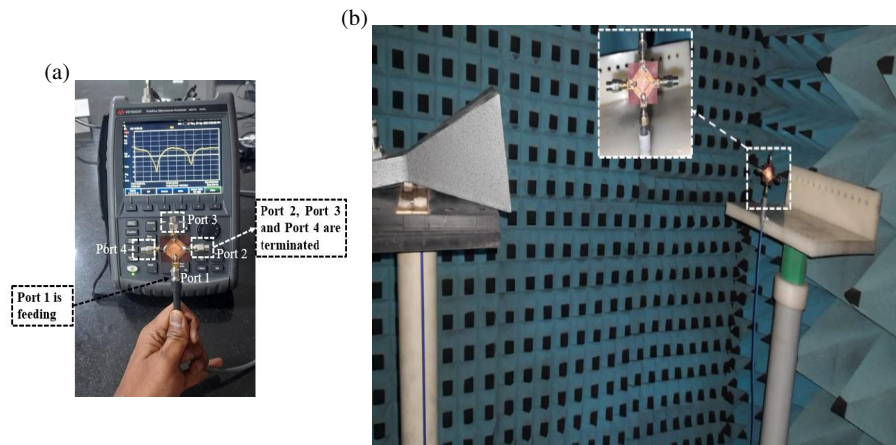


FIGURE 8. Measurement setup in anechoic chamber. (a) Measurements calculations in VNA. (b) Antenna under test setup.

## 4. RESULTS AND DISCUSSIONS

A dual-band rhombus-shaped MIMO patch (RSMP) antenna is designed and analyzed by using CST software. The proposed antenna resonates at multiple operating frequencies (12.9 GHz and 16.5 GHz) with a reflection coefficient of  $-17$  dB and  $-27.5$  dB. Also, it has two narrow bandwidths of 300 MHz (12.77 GHz to 13.07 GHz) and 350 MHz (16.31 GHz to 16.66 GHz). The fabricated prototype of the proposed RSMP antenna is shown in Figs. 7(a)–(b), and measurement setup is shown in Figs. 8(a)–(b). The operation and working principal modes of the proposed RSMP antenna is that when one port is

feeding the remaining three ports are terminated with 50 ohms matching stubs.

The simulated and measured  $E$ -plane and  $H$ -plane radiation patterns of each port, i.e.,  $P_1$ ,  $P_2$ ,  $P_3$ , and  $P_4$ , at 12.9 GHz and 16.5 GHz frequencies of the RSMP antenna are shown in Fig. 9. The co-polarization (co-pol) and cross-polarization ( $x$ -pol) for both the  $E$ - and  $H$ -planes are presented in Figs. 9(a)–(p) of the RSMP antenna at four ports for dual-bands. The maximum radiation of the major lobe exists at  $0^\circ$  and  $45^\circ$  in  $E$ -plane co-pol and  $x$ -pol. Similarly, maximum radiation exists at  $15^\circ$  and  $45^\circ$  in  $H$ -plane co-pol and  $x$ -pol.

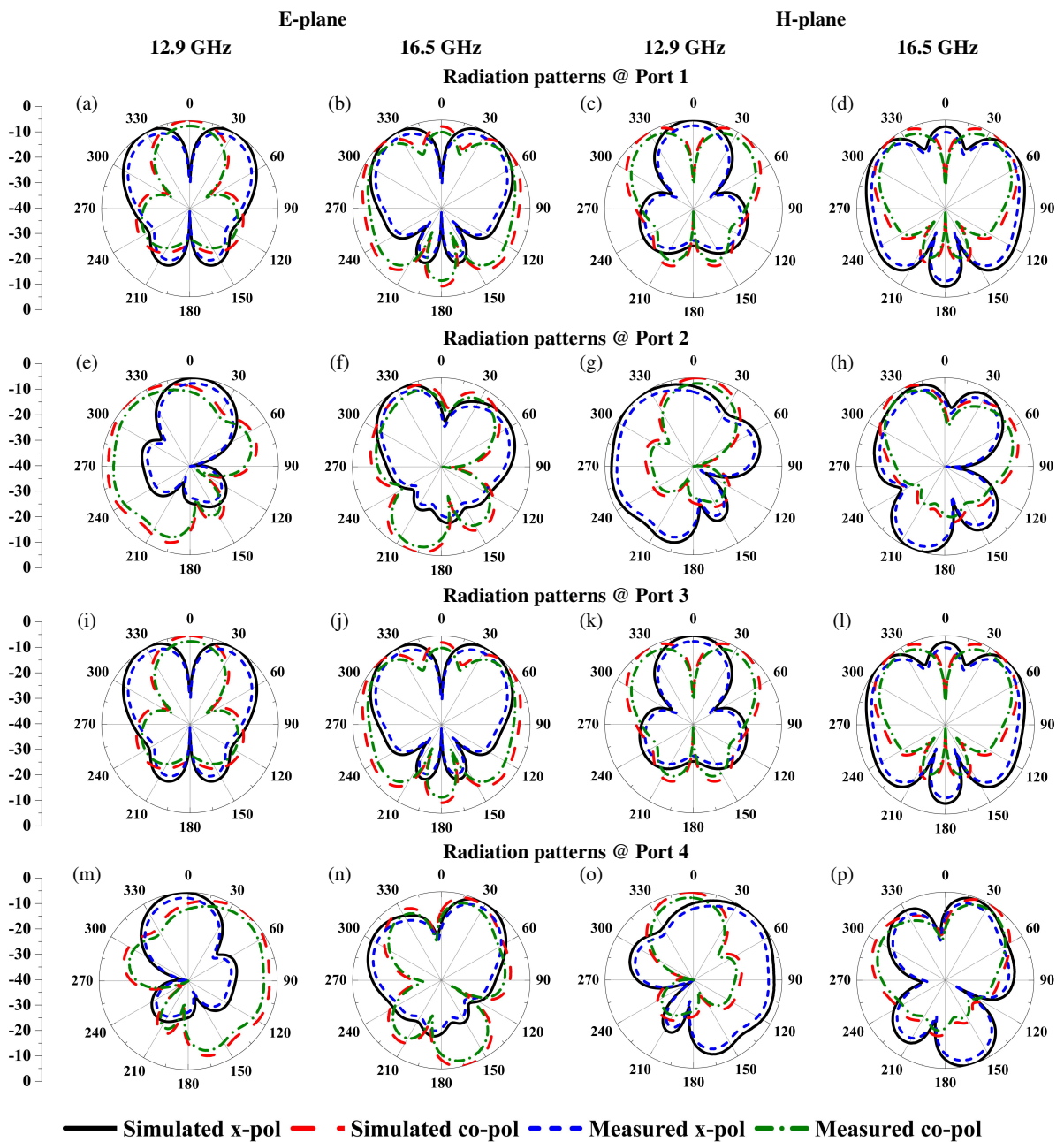


**FIGURE 9.** Radiation patterns of RSMP antenna, (a), (e), (i), (m) *E*-plane at 12.9 GHz, (b), (f), (j), (n) *E*-plane at 16.5 GHz, (c), (g), (k), (o) *H*-plane at 12.9 GHz, (d), (h), (l), (p) *H*-plane at 16.5 GHz.

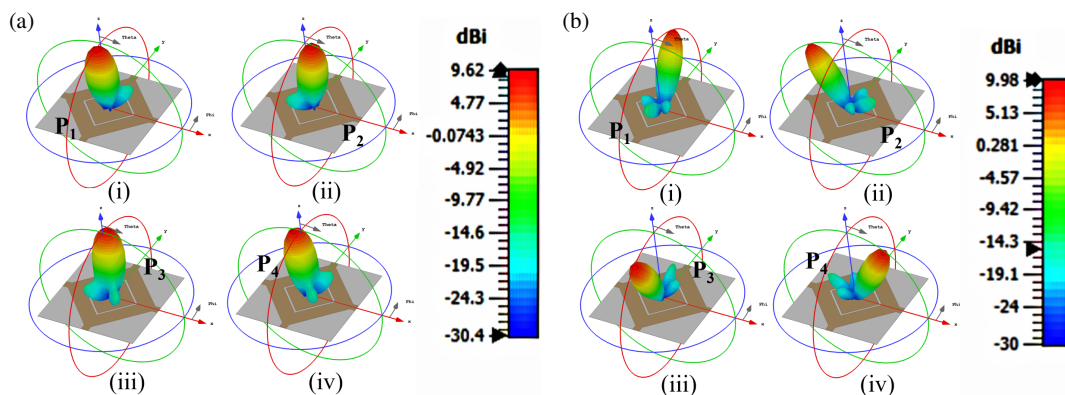


**FIGURE 10.** Gain plot of proposed MIMO antenna at (a) 12.9 GHz, (b) 16.5 GHz.

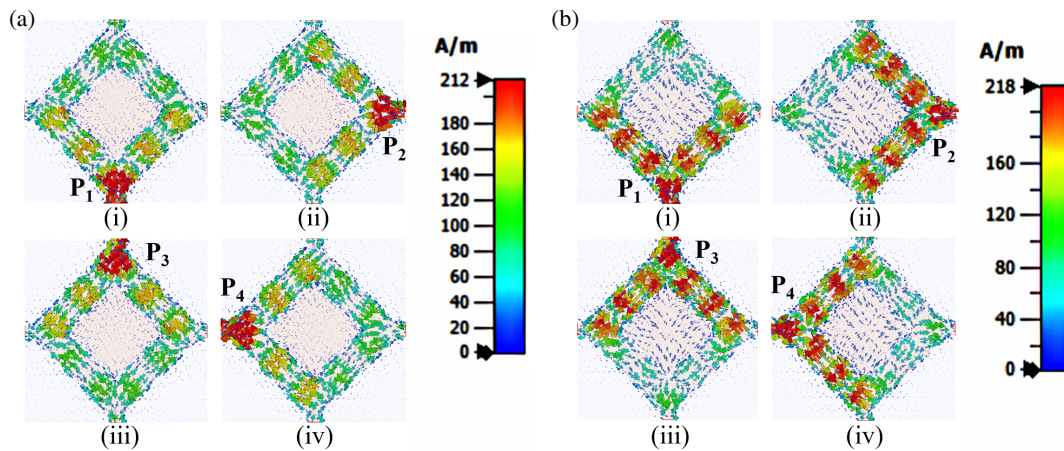


FIGURE 11. Surface current distribution at (a) 12.9 GHz, (b) 16.5 GHz.

TABLE 3. Comparison table of proposed antenna model with existing models.

Ref No.	Antenna Size (mm <sup>3</sup> )	Substrate Material	Resonating frequency (GHz)	Gain (dBi)
[1]	77 × 79 × 2.2	Rogers RO4350	12.4 14.2	8.0 8.2
[5]	10 × 80 × 1.524	TSM-DS3	16.5 33.2	6.8 6.9
[6]	58 × 58 × 0.76	Roger RO3003	12.4 14.6	7.5 8.7
[7]	50 × 30 × 0.787	Dielectric substrate	4.6	7.16
[15]	26 × 32 × 0.235	Flexible FR-4	3.58	6.8
Proposed	28 × 28 × 0.07	Polyimide	12.9 16.5	9.62 9.98

The gains observed in the proposed RSMP antenna at 12.9 GHz and 16.5 GHz operating frequencies are 9.62 dBi and 9.98 dBi for each port, i.e.,  $P_1$ ,  $P_2$ ,  $P_3$ , and  $P_4$ , and it is presented in Fig. 10. The direction of the main beam is also shown in the respective ports ( $P_1$ – $P_4$ ) of the operating frequencies in Figs. 10(a)–(b). Similarly, Fig. 11 shows the surface current distribution (SCD) excited at their respective ports ( $P_1$ – $P_4$ ) of resonant frequencies 12.9 GHz and 16.5 GHz. In Table 3 the comparisons of existing antennas to the proposed RSMP antenna is summarized. From this table, it is observed that the proposed RSMP antenna has more gain and less area.

## 5. CONCLUSION

In this paper, a compact quad-port rhombus-shaped patch antenna with a complete ground plane structure has been proposed. The symmetric nature of the rhombus shape is compared to the other shapes like rectangle, square, circle, triangle, etc. It provides stability, reduces interference, enhances the gain, and is also suitable for MIMO application in wireless communications. The proposed MIMO antenna design resonates at 12.9 GHz and 16.5 GHz with reflection coefficients of  $-17$  dB and  $-27$  dB, respectively. A rhombus-shaped slot is

etched from the common patch configuration used to generate high gain and dual-band frequencies. The maximum peak gains and bandwidths of the proposed MIMO antenna are 9.62 dBi, 9.98 dBi, 300 MHz, and 350 MHz at 12.9 GHz and 16.5 GHz, respectively. The simulated and measured results of antenna characteristics are presented, and they agree with each other. The proposed RSMP antenna MIMO parameters are observed for  $ECC < 0.2$ ,  $DG > 9.5$ , TARC, and  $CCL < 0.4$  bits/sec/Hz. The RSP antenna has dual bands, and it is well suited at Ku-band for broadcasting communications for the wireless communications.

## REFERENCES

- [1] Kong, L. and X. Xu, "A compact dual-band dual-polarized microstrip antenna array for MIMO-SAR applications," *IEEE Transactions on Antennas and Propagation*, Vol. 66, No. 5, 2374–2381, May 2018.
- [2] Lee, S. W. and Y. J. Sung, "Reconfigurable rhombus-shaped patch antenna with Y-shaped feed for polarization diversity," *IEEE Antennas and Wireless Propagation Letters*, Vol. 14, 163–166, 2015.
- [3] Sharma, N. and S. S. Bhatia, "Ultra-wideband fractal antenna using rhombus shaped patch with stub loaded defected ground

- plane: Design and measurement,” *AEU — International Journal of Electronics and Communications*, Vol. 131, 153604, Mar. 2021.
- [4] Saravanan, M. and M. J. S. Rangachar, “Design of rhombus-shaped slot patch antenna for wireless communications,” *Journal of Computer Networks and Communications*, Vol. 2019, 5149529, 2019.
- [5] Liu, S., K. Jiang, G. Xu, X. Ding, K. Zhang, J. Fu, and Q. Wu, “A dual-band shared aperture antenna array in Ku/Ka-bands for beam scanning applications,” *IEEE Access*, Vol. 7, 78 794–78 802, 2019.
- [6] Tang, H., C. J. Bulger, T. Rovere, B. Zheng, S. An, H. Li, Y. Dong, M. Haerinia, C. Fowler, S. Gonya, W. Guo, and H. Zhang, “A low-profile flexible dual-band antenna with quasi-isotropic radiation patterns for MIMO system on UAVs,” *IEEE Antennas and Wireless Propagation Letters*, Vol. 22, No. 1, 49–53, Jan. 2023.
- [7] Cheng, B. and Z. Du, “A wideband low-profile microstrip MIMO antenna for 5G mobile phones,” *IEEE Transactions on Antennas and Propagation*, Vol. 70, No. 2, 1476–1481, Feb. 2022.
- [8] Ambalgi, A. P., S. K. Sujata, and A. Vaish, “Experimental and simulation study of effects in etched patch antenna with multi slots,” *WSEAS Transactions on Communications*, Vol. 19, 142–148, 2020.
- [9] Pasumarthi, S. R., J. B. Kamili, and M. P. Avala, “Design of dual band MIMO antenna with improved isolation,” *Microwave and Optical Technology Letters*, Vol. 61, No. 6, 1579–1583, Jun. 2019.
- [10] Wang, H., R. Zhang, Y. Luo, and G. Yang, “Compact eight-element antenna array for triple-band MIMO operation in 5G mobile terminals,” *IEEE Access*, Vol. 8, 19 433–19 449, 2020.
- [11] Chattha, H. T., M. K. Ishfaq, B. A. Khawaja, A. Sharif, and N. Sheriff, “Compact multiport MIMO antenna system for 5G IoT and cellular handheld applications,” *IEEE Antennas and Wireless Propagation Letters*, Vol. 20, No. 11, 2136–2140, Nov. 2021.
- [12] Li, Z., C. Yin, and X. Zhu, “Compact UWB MIMO Vivaldi antenna with dual band-notched characteristics,” *IEEE Access*, Vol. 7, 38 696–38 701, 2019.
- [13] Choi, J., W. Hwang, C. You, B. Jung, and W. Hong, “Four-element reconfigurable coupled loop MIMO antenna featuring LTE full-band operation for metallic-rimmed smartphone,” *IEEE Transactions on Antennas and Propagation*, Vol. 67, No. 1, 99–107, Jan. 2019.
- [14] Ikram, M., E. A. Abbas, N. Nguyen-Trong, K. H. Sayidmarie, and A. Abbosh, “Integrated frequency-reconfigurable slot antenna and connected slot antenna array for 4G and 5G mobile handsets,” *IEEE Transactions on Antennas and Propagation*, Vol. 67, No. 12, 7225–7233, Dec. 2019.
- [15] Desai, A., J. Kulkarni, M. M. Kamruzzaman, S. Hubálovský, H.-T. Hsu, and A. A. Ibrahim, “Interconnected CPW fed flexible 4-port MIMO antenna for UWB, X, and Ku band applications,” *IEEE Access*, Vol. 10, 57 641–57 654, 2022.
- [16] Dey, S., S. Dey, and S. K. Koul, “Isolation improvement of MIMO antenna using novel EBG and hair-pin shaped DGS at 5G millimeter wave band,” *IEEE Access*, Vol. 9, 162 820–162 834, 2021.
- [17] Hannan, S., M. T. Islam, N. M. Sahar, K. Mat, M. E. H. Chowdhury, and H. Rmili, “Modified-segmented split-ring based polarization and angle-insensitive multi-band metamaterial absorber for X, Ku and K band applications,” *IEEE Access*, Vol. 8, 144 051–144 063, 2020.
- [18] Yang, W. J., Y. M. Pan, and S. Y. Zheng, “Mutual coupling reduction in CP MIMO crossed-dipole antenna array,” *IEEE Antennas and Wireless Propagation Letters*, Vol. 21, No. 12, 2442–2446, Dec. 2022.
- [19] Krishna, O. N. V. R. and K. K. Naik, “Analysis of triangular antenna with two annular rings for multi-band applications,” *Journal of Critical Reviews*, Vol. 7, No. 4, 189–191, 2020.
- [20] Amala Vijaya Sri, P., G. Srikanth, B. V. Krishna, K. Kousalya, S. R. Lavanya, K. Ooha, R. P. S. Chaitanya, B. K. Kumar, K. Y. Srinivas, and K. K. Naik, “Enhancement of gain with coplanar isosceles triangular patch antenna for dual-band applications,” in *2017 Progress In Electromagnetics Research Symposium — Fall (PIERS — FALL)*, 2981–2984, Singapore, Nov. 2017.